Temperature Estimation of Partially Shaded Photovoltaic Modules Using a Multiphysics Model

Yu Shen, Zhen Xu, Yiye Wang, Chenxi Li, Jinxia Zhang, Kanjian Zhang, and Haikun Wei

***Abstract*—Partial shading is common in both photovoltaic (PV) stations and building integrated PV systems. The temperature increase of partially shaded (PTS) module not only reduces its efficiency but also accelerates its degradation. Therefore, temperature estimation of PTS module is essential for assessment and maintainence of PV systems. In this article, a multiphysics model consisting of an electrical model, an optical model, and a thermal model is developed. Particularly, the parallel circuit is adopted for the PTS cell, making it possible to calculate the electric power and heat generation of shaded region and unshaded region in the PTS cell, respectively. To the best of our knowledge, it is the first attempt to estimate the temperature distribution of PV module with PTS cell. Experiments are conducted on monocrystalline PV modules. One specific cell is partially shaded in various proportions and environmental conditions. The maximum temperature on the front surface of the PTS module is measured with the infrared thermographic camera and also calculated by our method. The root mean square error is 6.14 °C, which verifies the effectiveness of the proposed multiphysics model for temperature estimation of PTS modules.**

***Index Terms*—Multiphysics model, PV module, parallel circuit, partially shaded, temperature estimation.**

I. Introduction

ON ACCOUNT of the increasing efficiency and declining cost, the photovoltaic (PV) modules' installation has been growing rapidly in recent years [1]. The partial shading conditions are common cases in PV station due to shadow [2], soil [3], dust [4], bird droppings [5], and leaves. The high-density planning of building integrated photovoltaics also lead to partial shading conditions [6]. Several scientific observations showed that the temperature of partially shaded (PTS) module might increase dramatically. Clement [7] shaded one specific cell at the ratio from 0% to 100% under standard testing condition (STC). The maximum temperature, which was measured with an infrared thermographic camera, ranged from 56 °C to 136 °C. In [8], the surface temperature of PV module reached above 140 °C under partial shading conditions.

The temperature has a great impact on the electrical characteristics, lifetime, and safety of PV module [9]. On the one hand, the electrical characteristics of PV module is related to its cell temperature [10]. When the cell temperature increases by 1 °C, its efficiency will decrease by 0.5% approximately [11]. On the other hand, the temperature increase may accelerate the degradation of PV modules and reduce their lifetime [12]. Irreversible destruction of silicon structure in the overheated cell was observed with the scanning electron microscopy [13]. The thermomechanical stress [14] between the shaded region and unshaded region in the PTS cell may degrade this cell and result in hot spot [15]. The temperature increase of the PTS module may cause browning, burn marks or, in the worst case, fire [16]. Therefore, it is necessary to estimate the temperature of PTS modules.

In some literature, a simple approach to calculate the temperature of PV module expresses the cell temperature as an empirical function of environmental variables [17]–[19]. However, this method only applies to PV modules under homogeneous conditions. Another way to estimate the temperature of PV module is considering the energy conversion mechanism between the PV module and the environment [20]–[22]. In [23], an optical model was adopted to calculate the absorbed solar power of each layer in the PV module. Siddiqui [24] developed a 3-D thermal model and solved it by the finite element software. These studies estimated the heat generation of silicon cell by its absorbed solar power and electrical efficiency. However, the electrical efficiency of the silicon cell might change a lot when the PV module is partially shaded. An electrical model is necessary to analyze the electric power of each cell in the PTS module.

A multiphysics model was presented in [25] for the transient analysis of electrical, thermal, and structural performance of PV module. Subsequently, Li [26] used a multiphysics model to estimate the temperature of building integrated PV modules under shading conditions. However, these existing methods roughly calculated the electric power and heat generation of the entire cell, which did not separately measure the shaded and unshaded regions in the same cell. There is a great difference in temperature between shaded and unshaded region in the PTS cell [27]. Estimating the electric power and heat generation of shaded and unshaded region in the PTS cell, respectively,

Manuscript received 19 January 2022; revised 20 April 2022; accepted 13 May 2022. Date of publication 14 June 2022; date of current version 19 August 2022. This work was supported in part by the National Key Research and Development Program of China under Grant 2018YFB1500800, in part by the National Natural Science Foundation of China under Grant 61773118, Grant 61703100, and Grant 61973083, and in part by the Science and Technology Project of State Grid Corporation of China (Intelligent operation and maintenance technology of distributed photovoltaic system SGTJDK00DYJS2000148). *(Corresponding authors: Jinxia Zhang; Haikun Wei.)*

The authors are with the Key Laboratory of Measurement and Control of CSE Ministry of Education and School of Automation, Southeast University, Nanjing 210096, China (e-mail: 230169411@seu.edu.cn; zxu@seu.edu.cn; wangyiye@seu.edu.cn; chenxi_li@seu.edu.cn; jinxiazhang@seu.edu.cn; kjzhang@seu.edu.cn; hkwei@seu.edu.cn).

Color versions of one or more figures in this article are available at https://doi.org/10.1109/JPHOTOV.2022.3176440.

Digital Object Identifier 10.1109/JPHOTOV.2022.3176440

is necessary but has never been considered. This means that existing temperature estimation approaches can hardly apply to PTS modules. The thermal performance of PTS modules has rarely been investigated.

In light of the above, a multiphysics model is developed in this article to estimate the temperature distribution of PTS module. This multiphysics model consists of an electrical model, an optical model, and a thermal model. Particularly, in the electrical model, the physically explicable parallel circuit [28] is adopted to analyze the electric power of shaded region and unshaded region in the PTS cell, respectively. Combining the electrical model and the optical model, heat generation of shaded and unshaded region in the PTS cell can also be calculated, respectively. The thermal model, considering heat generation and heat transfer, is solved by the finite element method. To the best of our knowledge, it is the first attempt to estimate the temperature distribution of PTS module, which can explain the temperature difference between shaded region and unshaded region in the PTS cell. Experiments are conducted on the monocrystalline PV module with area-measurable shade cloth. An individual cell in the PV module is partially shaded with fixed proportion for a continuous period of time on a sunny day. In addition, one specific cell in the PV module is partially shaded in various proportions and environmental conditions. These experimental results verify the effectiveness of the proposed method for temperature perdiction of PTS modules. Compared with direct temperature measurement, the proposed method can easily obtain the temperature distribution of PV modules under different shading conditions and different environmental conditions. This method can estimate not only the surface temperature of the PTS module, but also the internal temperature of each cell. Furthermore, the structure model can join the proposed multiphysics model to analyze the thermomechanical stress of the PTS cell.

The rest of this article is organized as follows. The multiphysics model is described in Section II. Next, experiments and results are presented in Section III. Subsequent to this, some interesting observations are discussed in Section IV. Finally, Section V concludes this article.

II. Proposed Multiphysics Model

In this section, a multiphysics model is proposed to estimate the temperature distribution of PTS modules. The overall framework of the multiphysics model is shown in Fig. 1. First, the electrical model is proposed to analyze the electric power of each cell, which is described in Section II-A. And then, the optical model is combined to calculate the absorbed solar power of each layer in the PTS module, which is introduced in Section II-B. Finally, the thermal model, considering heat generation and heat transfer of the PTS module, is solved by the finite element method in Section II-C.

A. Electrical Model

Generally, the electrical model of PV module is composed of three substrings, as shown in Fig. 2. Each substring usually consists of several silicon cells connected in series, protected

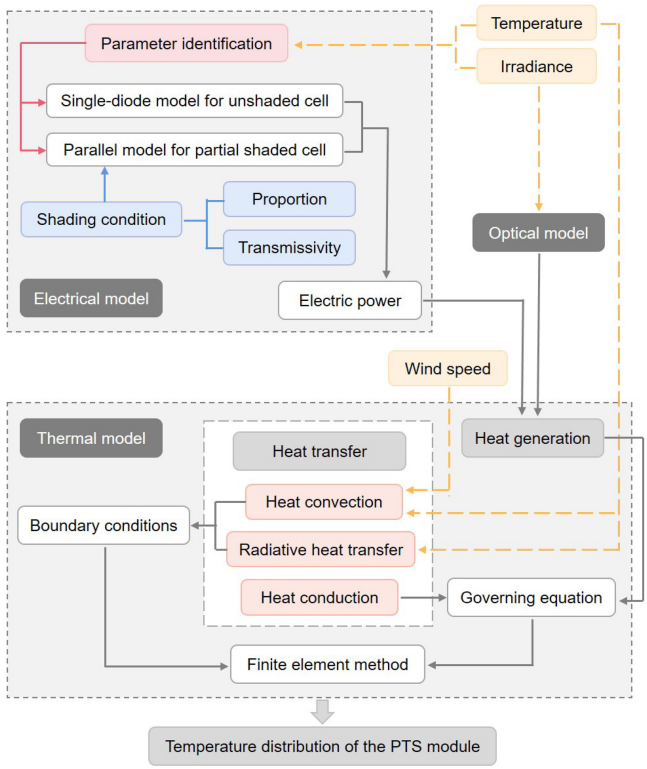

Fig. 1. The overall framework of the multi-physics model.

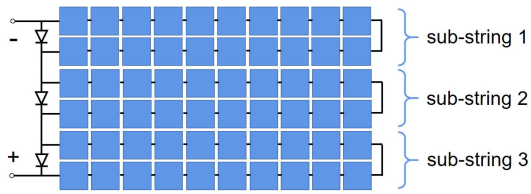

Fig. 2. Electrical model of PV module.

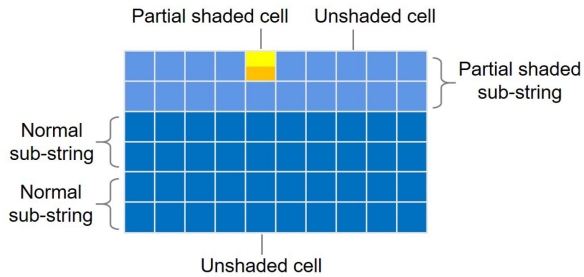

Fig. 3. Silicon cells behave differently in the PTS module.

with a bypass diode. Silicon cells behave differently in the PTS module, as shown in Fig. 3. The temperature of unshaded region in the PTS cell increase significantly while the temperature of shaded region increase slightly. The temperature distribution of unshaded cell is almost uniform.

1) Single-Diode Model for Unshaded Cell: For unshaded cells, the single-diode model (SDM) [29] is used to describe their *I–V* characteristics, as shown in Fig. 4. SDM has five parameters consisting of the photoinduced current I_{ph}, the shunt resistance

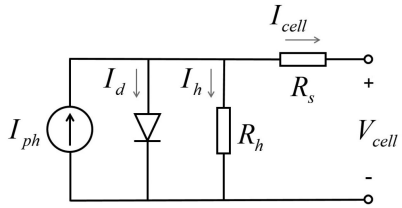

Fig. 4. Single-diode model.

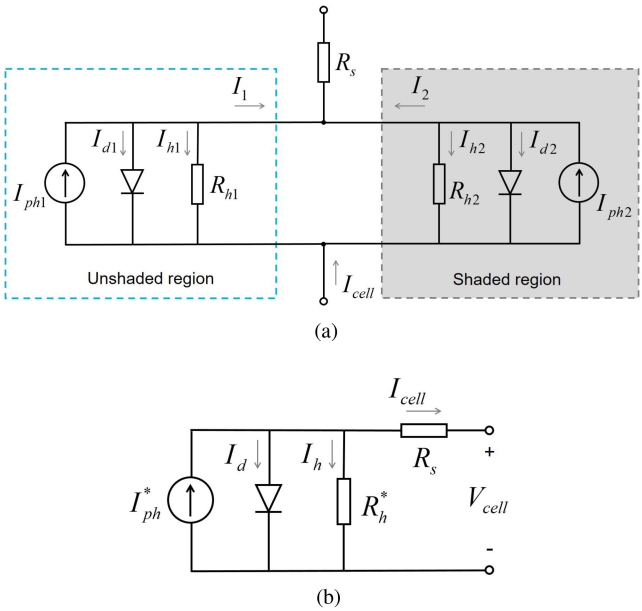

Fig. 5. Parallel circuit and its equivalent SDM for the PTS cell. (a) The parallel circuit. (b) The equivalent SDM.

R_h, the series resistance R_s, the reverse saturation current I_s, and the ideality factor n of the diode. Parameter identification of SDM is described in [30].

The relationship between the current I_{cell} and voltage V_{cell} is shown by the following nonlinear equation [29]:

$$I_{\text{cell}} = I_{ph} - I_s \left[\exp\left(\frac{V_{\text{cell}} + I_{\text{cell}} \cdot R_s}{n \cdot V_T}\right) - 1\right] - \frac{V_{\text{cell}} + I_{\text{cell}} \cdot R_s}{R_h} \tag{1}$$

where the thermal voltage V_T [29] is defined as follows:

$$V_T = \frac{k \cdot T_c}{q} \tag{2}$$

where k is the Boltzmann constant (1.38×10^{-23}J/K), q is the electron charge (1.60×10^{-19}C), and T_c is the cell temperature.

2) The Parallel Circuit for the PTS Cell: For the PTS cell, the parallel circuit [28] is adopted, as shown in Fig. 5(a). The blue dotted box represents the unshaded region and the gray box represents the shaded region. Its equivalent SDM is shown in Fig. 5(b).

The ratio of irradiance passing through certain material depends on its transmissivity. The transmittance of different materials varies. Given the transmittance tr of the shading object and the shading proportion $p\%$, the photoinduced current of unshaded region and shaded region in Fig. 5(a) are calculated by (3) and (4) respectively,

$$I_{ph1} = I_{ph} \cdot (1 - p\%) \tag{3}$$

$$I_{ph2} = I_{ph} \cdot tr \cdot p\% \tag{4}$$

where I_{ph} is the photoinduced current of SDM.

The photoinduced current I^*_{ph} in Fig. 5(b) is calculated in

$$I^*_{ph} = I_{ph1} + I_{ph2}. \tag{5}$$

The shunt resistance R_{h1} and R_{h2} in Fig. 5(a) are calculated in (6) and (7), respectively,

$$R_{h1} = \frac{R_h}{(1 - p\%)} \tag{6}$$

$$R_{h2} = \frac{R_{h,\text{shade}}}{p\%} \tag{7}$$

where R_h is the shunt resistance of SDM, and $R_{h,\text{shade}}$ is the shunt resistance of the shaded cell, which is calculated in

$$R_{h,\text{shade}} = \frac{1}{tr} \cdot R_h. \tag{8}$$

The shunt resistance R^*_h in Fig. 5(b) is calculated in

$$R^*_h = \frac{R_{h1} \cdot R_{h2}}{R_{h1} + R_{h2}}. \tag{9}$$

3) Electric Power: Given the current I_{pv} of the PTS module, the current of each substring is available

$$I_{\text{sub}} = I_{pv}. \tag{10}$$

The current of cells in the substring is calculated in

$$I_{\text{cell}} = \begin{cases} I_{\text{sub}}, & \text{if } (I_{\text{sub}} \leqslant I_{\text{cell,max}}) \\ I_{\text{cell,max}}, & \text{if } (I_{\text{sub}} \geqslant I_{\text{cell,max}}) \end{cases} \tag{11}$$

where the maximum current of solar cells $I_{\text{cell,max}}$ in the substring can be obtained when V_{sub} described in (13) reduced to $-V_{th}$ as the current of substring I_{sub} increases.

Based on the SDM for unshaded cell and the parallel circuit for the PTS cell, the voltage of the ith cell in the substring is calculated in

$$V_{\text{cell,i}} = \begin{cases} n \cdot V_T \cdot \ln\left(\frac{I_{ph,i} - I_{\text{cell}}}{I_s} + 1\right) - I_{\text{cell}} \cdot R_s, \\ \qquad \text{if } (I_{\text{cell}} \leqslant I_{ph,i}) \\ -(I_{\text{cell}} - I_{ph,i}) \cdot R_{h,i} - I_{\text{cell}} \cdot R_s, \\ \qquad \text{if } (I_{\text{cell}} \geqslant I_{ph,i}) \end{cases} \tag{12}$$

where $I_{ph,i}$ is the photoinduced current of the ith cell, $R_{h,i}$ is the shunt resistance of the ith cell, and I_{cell} is the current of solar cells in the substring.

The voltage of the substring is calculated in

$$V_{\text{sub}} = \begin{cases} \sum_1^M V_{\text{cell,i}}, & \text{if } \left(\sum_1^M V_{\text{cell,i}} \geqslant -V_{th}\right) \\ -V_{th}, & \text{if } \left(\sum_1^M V_{\text{cell,i}} \leqslant -V_{th}\right) \end{cases} \tag{13}$$

where M is the number of cells in the substring, and V_{th} is the threshold when the bypass diode of the substring is conducting ($V_{th} = 0.7$ V for silicon).

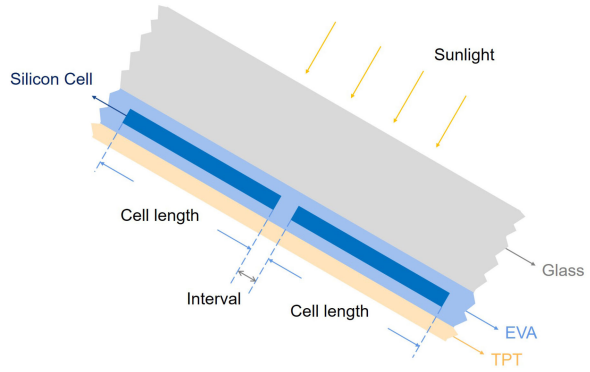

Fig. 6. Sketch map (partly) of the PV module from the side view.

The electric power of each cell is calculated in

$$P_{\text{electric}} = I_{\text{cell}} \cdot V_{\text{cell}}. \tag{14}$$

For the PTS cell, the electric power of unshaded region and shaded region is estimated, respectively, as follows. The current of the diode in the equivalent SDM shown in Fig. 5(b) is calculated in

$$I_d = I_s \left[\exp\left(\frac{V_{\text{cell}} + I_{\text{cell}} \cdot R_s}{n \cdot V_T} \right) - 1 \right]. \tag{15}$$

The current I_{d1} and I_{d2} in Fig. 5(a) are calculated in the following:

$$I_{d1} = I_d \cdot (1 - p\%) \tag{16}$$

$$I_{d2} = I_d \cdot p\%. \tag{17}$$

The current I_{h1} and I_{h2} in Fig. 5(a) are calculated in the following:

$$I_{h1} = \frac{V_{\text{cell}} + I_{\text{cell}} \cdot R_s}{R_{h1}} \tag{18}$$

$$I_{h2} = \frac{V_{\text{cell}} + I_{\text{cell}} \cdot R_s}{R_{h2}}. \tag{19}$$

The current I_1 of unshaded area is calculated in (20) and the current I_2 of shaded area is calculated in (21)

$$I_1 = I_{ph1} - I_{d1} - I_{h1} \tag{20}$$

$$I_2 = I_{ph2} - I_{d2} - I_{h2}. \tag{21}$$

The electric power $P_{\text{electric},1}$ of unshaded area in the PTS cell is calculated in (22) and the electric power $P_{\text{electric},2}$ of shaded area is calculated in (23)

$$P_{\text{electric},1} = I_1 \cdot V_{\text{cell}} \tag{22}$$

$$P_{\text{electric},2} = I_2 \cdot V_{\text{cell}}. \tag{23}$$

B. Optical Model

The PV module consists of glass cover, ethylene vinyl acetate (EVA) layer, silicon cells, and Tedlar/PET/Tedlar (TPT) backsheet [23]. The cross-sectional view of PV module is shown in Fig. 6.

The solar power arriving at the PV module is partly reflected while mostly absorbed. The absorbed solar power of silicon cell layer is converted into electricity and heat, while the absorbed solar power of other layers totally turns into heat.

TABLE I
OPTICAL PROPERTIES AND THICKNESS OF MATERIALS IN THE PV MODULE

Material	Reflectivity	Absorptivity	Transmissivity	Thickness
Glass	4%	4%	92%	3.20 mm
EVA	2%	8%	90%	0.42 mm
Silicon Cell	8%	90%	2%	0.18 mm
TPT (Polymer)	86%	12.8%	1.2%	0.18 mm

The solar power absorbed by the glass cover, EVA, Silicon cell, and TPT per unit volume [23] can be calculated in

$$Q_j = \frac{G \cdot \alpha_j \cdot \beta_j}{d_j} \tag{24}$$

where G is the solar irradiance, α_j is the absorptivity of the jth layer, β_j is the product of all prelayers' transmissivity, and d_j is the thickness of the jth layer. The optical properties and thickness of these materials [23] are shown in Table I.

C. Thermal Model

The temperature distribution of the PV module is estimated based on the following hypotheses:

1) The PV module is at steady state, which means that its temperature distribution does not change over time.
2) The ambient temperature surrounding the PV module is uniform.
3) Thermal properties of materials in the PV module are isotropic and temperature-independent.
4) Solar irradiance arriving at the metallization and interconnect ribbons is neglected.

1) Heat Generation: The heat generation of glass, EVA, and TPT in Fig. 6 can be considered as their absorbed solar power. However, the absorbed solar power of silicon cell is converted into electricity and heat. Therefore, the heat generation of each cell per unit volume is calculated in

$$Q_{\text{heat}} = Q_{\text{silicon}} - \frac{P_{\text{electric}}}{v} \tag{25}$$

where v is the volume of silicon cell.

For the PTS cell, the heat generation of unshaded region and shaded region per unit volume is calculated in (26) and (27), respectively. It can be derived that the heat generation of the unshaded region per unit volume is higher than the shaded region for the PTS cell

$$Q_{\text{heat},1} = Q_{\text{silicon},1} - \frac{P_{\text{electric},1}}{v \cdot (1 - p\%)} \tag{26}$$

$$Q_{\text{heat},2} = Q_{\text{silicon},2} - \frac{P_{\text{electric},2}}{v \cdot p\%} \tag{27}$$

2) Heat Transfer: Heat transfer of PTS module consists of heat conduction, heat convection, and radiative heat transfer. Since the thickness of PV module is much smaller compared with its length and width, as shown in Table II, the heat transfer on the side of PV module is ignored. Heat convection and radiative heat transfer occur both on the front and back surface of PV module, as shown in Fig. 7.

TABLE II
SIZE OF THE PV MODULE

Length (mm)	Width (mm)	Thickness (mm)
1650	992	35

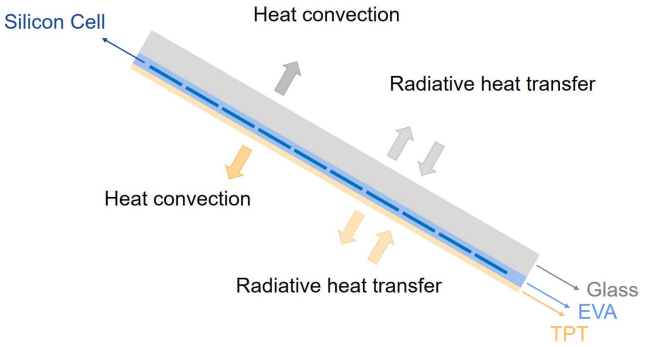

Fig. 7. Heat convection and radiative heat transfer of PV module.

TABLE III
THERMAL PROPERTIES OF MATERIALS IN THE PV MODULE

Material	Emissivity	Thermal conductivity (W/m K)
Glass	0.85	2.00
EVA	-	0.31
Silicon Cell	-	130.00
TPT (Polymer)	0.9	0.15

Heat convection is described by Newton's law of cooling [31], as shown in

$$\Phi_{\text{convection}} = hS\Delta T \tag{28}$$

where h is the convective heat transfer coefficient, S is the surface area, and ΔT represents the temperature difference between the surface temperature and the air temperature.

The convective heat transfer coefficient at the front and back surface of PV module [32] is calculated as

$$h = 5.82 + 4.07 \cdot w \tag{29}$$

where w is the wind speed.

Radiative heat transfer is described by Stefan–Boltzmann law [31], as shown in

$$\Phi_{\text{radiation}} = \varepsilon S\sigma T^4 \tag{30}$$

where ε is the emissivity, S is the surface area, σ is the Stefan–Boltzmann constant which is equal to 5.67×10^{-8} W/(m$^2 \cdot$ K^4), and T represents the temperature.

The front and back surfaces of the PV module are considered to view the sky and ground, respectively. The temperature of sky is assumed to be ambient temperature. The emissivity of the glass cover and TPT backsheet are shown in Table III.

Heat conduction is described by the Fourier's law [31], and the governing equation of 3-D heat conduction at steady state is shown in

$$\lambda\left(\frac{\partial^2 T}{\partial x^2} + \frac{\partial^2 T}{\partial y^2} + \frac{\partial^2 T}{\partial z^2}\right) + Q = 0 \tag{31}$$

where λ is the thermal conductivity, which is listed in Table III; Q is the heat generation.

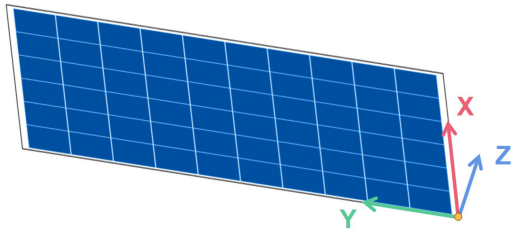

Fig. 8. Geometry of the PV module.

TABLE IV
STRUCTRAL INFORMATION OF SILICON CELLS IN THE PV MODULE

Cell size	Cell interval	Cell number	Margin	
			Long edge	Short edge
156 × 156 mm^2	2 mm	6 × 10	35 mm	22 mm

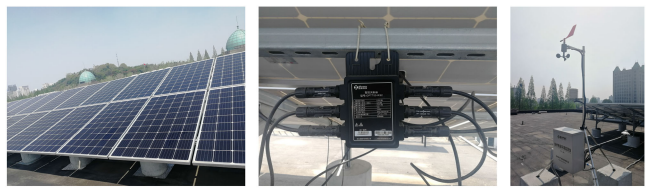

(a) (b) (c)

Fig. 9. Experimental equipment: (a) monocrystalline modules; (b) PV module monitoring device; and (c) environment monitoring recorder.

3) Finite Element Method: FEM is adopted to solve the governing equation shown in (31). The PV module is discretized into finite elements and nodes. Then, the nodal temperature is calculated and the temperature distribution of the PV module is obtained by interpolation. Boundary conditions are set as heat convection and radiative heat transfer on the front and back surface of PV module.

ANSYS workbench is utilized to deal with the steady-state thermal system. The geometry of PV module is shown in Fig. 8 and the structural information of silicon cells is listed in Table IV.

III. EXPERIMENTS AND RESULTS

Experiments are conducted on monocrystalline PV modules to evaluate the performance of the proposed method. Details of data collection are described in Section III-A, and then performance evaluation is shown in Section III-B.

A. Data Collection

Shading experiments are conducted on monocrystalline PV modules (STP 310S-20/Wfw), as shown in Fig. 9(a). The characteristics of the PV modules are shown in Table V. Every two PV modules are connected to a monitoring device (OPT700-RS), as shown in Fig. 9(b). The monitoring devices are used to measure the current and voltage of each PV module. The global solar irradiance of the plane parallel to PV modules is measured with a pyranometer (TBQ-2). The ambient temperature is measured with a temperature and humidity sensor (PTS-3). The wind parallel to the horizontal plane is measured with a wind speed and direction sensor (EC-8SX). These meteorological data are

TABLE V
CHARACTERISTICS OF THE PV MODULE

Characteristics	STC	NOCT
Maximum Power (Pmax)	310 W	228.7 W
Optimum Operating Voltage (Vmp)	33.4 A	30.6 V
Optimum Operating Current (Imp)	9.29 A	7.47 A
Open Circuit Voltage (Voc)	40.2 V	37.0 V
Short Circuit Current (Isc)	9.77 A	7.91 A
Temperature Coefficient of Voc	-0.34 %/°C	
Temperature Coefficient of Isc	0.060 %/°C	
Number of bypass diodes	3	

TABLE VI
OPTICAL PROPERTIES AND THICKNESS OF SHADE CLOTH

Reflectivity	Absorptivity	Transmissivity	Thickness
45%	50%	5%	0.08 mm

TABLE VII
THERMAL PROPERTIES OF SHADE CLOTH

Emissivity	Thermal conductivity (W/m K)
0.7	215

recorded with an environment monitoring recorder (TRM-ZSA) and user accessible with a software (PC-4). The environment monitoring recorder is shown in Fig. 9(c).

The angle between the surface of the PV module and the horizontal plane is 15°. Therefore, the wind vector should be decomposed into a component parallel to the surface of the PV module and a component perpendicular to the surface of the PV module. Since the PV modules used in the experiments are installed on the roof, we assume that the surface of the roof is horizontal and the wind speed perpendicular to the horizontal plane is zero. The wind speed along the short edge and long edge of the PV module is calculated as w_s and w_l, respectively,

$$w_s = w_m \cdot |\sin(\theta)| \tag{32}$$

$$w_l = w_m \cdot |\cos(\theta) \cdot \cos(\alpha)| \tag{33}$$

where w_m is the measured wind speed, θ is the wind direction, and α is the angle between the surface of the PV module and the horizontal plane.

Then, the wind speed parallel to the surface of PV modules is calculated as w, which is used to estimate the convective heat transfer coefficient

$$w = \sqrt{w_s^2 + w_l^2}. \tag{34}$$

PV modules are shaded by area-measurable shade cloth with regular shape. The shade cloth is assumed to be in seamless contact with the surface of glass cover. When analyzing the heat transfer of the shaded region, the optical properties, thickness, and thermal properties of shade cloth all need to be taken into consideration, which are listed in Table VI and Table VII, respectively.

The visible image is shown in Fig. 10(a). In order to achieve steady state, it is necessary to wait at least 10 min before measurement at each shading condition. The temperature of the PV module is measured with the thermographic camera (FLIR ONE Pro). Specifications of the thermographic camera are listed in Table VIII. The infrared thermal images are collected from

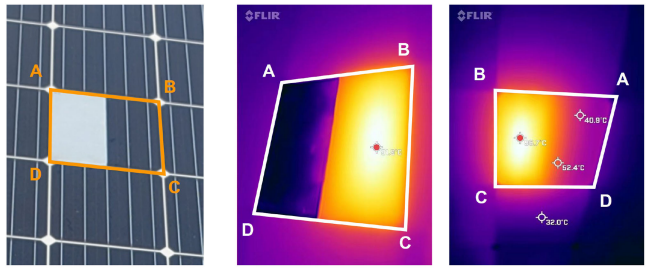

(a) (b) (c)

Fig. 10. Visible and infrared thermal images of PTS module: (a) visible image; (b) infrared thermal image from the front side; and (c) infrared thermal image from the back side. The PTS cell is labelled within the orange bounding box in the visible image and within the white bounding boxes in the infrared thermal images. The corners of the PTS cell are denoted as A, B, C and D.

TABLE VIII
SPECIFICATIONS OF THE THERMOGRAPHIC CAMERA (FLIR ONE PRO)

Items	Specifications
Thermal Resolution	160 × 120
Thermal Sensor	8 to 14 μm spectral range
Accuracy	± 3 °C
Object Temperature Range	-20 °C to 120 °C
Operating Temperature	0 °C to 35 °C

the front side of the PTS module, as shown in Fig. 10(b). The emissivity of the shade cloth is much lower than that of the glass cover on PV modules. As a result, the measured temperature of the shade cloth in the infrared thermal image is much lower than its actual temperature. To avoid this problem, only the maximum temperature of the unshaded region from the front side is used to evaluate the performance of the proposed method. In order to show the temperature difference between the shaded region and unshaded region in the PTS cell, a few infrared thermal images from the back side are also collected, as shown in Fig. 10(c).

In addition, the comparison between the temperature measured with the infrared thermal camera and a temperature sensor (PTWD-2 A) in direct contact with the PV module has been carried out. The PV module is disconnected during calibration experiments.

We have conducted 50 pairs of measurements from the back side and also 50 pairs of measurements from the front side. For the jth pair ($j = 1, 2, \cdots, 50$), the emissivity correction coefficients of TPT and glass are calculated as $c_{j,\text{back}}$ and $c_{j,\text{front}}$, respectively,

$$c_{j,\text{back}} = \frac{T_{s,j,\text{back}}^4}{T_{i,j,\text{back}}^4} \tag{35}$$

$$c_{j,\text{front}} = \frac{T_{s,j,\text{front}}^4}{T_{i,j,\text{front}}^4} \tag{36}$$

where $T_{s,j,\text{back}}$ is the temperature measured with the sensor in direct contact with the module for the jth calibration experiment from the back side, $T_{i,j,\text{back}}$ is the temperature measured with the infrared thermal camera for the jth calibration experiment from the back side, $T_{s,j,\text{front}}$ is the temperature measured with the sensor in direct contact with the module for the jth calibration experiment from the front side, and $T_{i,j,\text{front}}$ is the temperature

measured with the infrared thermal camera for the jth calibration experiment from the front side.

The emissivity of TPT and glass is corrected by c_b and c_f, respectively

$$c_b = \overline{c_{j,\text{back}}} \tag{37}$$

$$c_f = \overline{c_{j,\text{front}}}. \tag{38}$$

Then, the temperature measured with the infrared thermal camera from the back side and front side is calibrated as $T_{c,\text{back}}$ and $T_{c,\text{front}}$, respectively

$$T_{c,\text{back}} = \sqrt[4]{c_b} \cdot T_{i,\text{back}} \tag{39}$$

$$T_{c,\text{front}} = \sqrt[4]{c_b} \cdot T_{i,\text{front}} \tag{40}$$

where $T_{i,\text{back}}$ is the temperature measured with the infrared thermal camera from the back side, and $T_{i,\text{front}}$ is the temperature measured with the infrared thermal camera from the front side.

B. Performance Evaluation

In order to evaluate the performance of the proposed method, an individual cell in the PV module is partially shaded with fixed proportion for a continuous period of time on a sunny day. In addition, one specific cell in the PV module is partially shaded in various proportions and environmental conditions.

The electrical model of the PTS module has been validated in [28], which verifies that the modeling *I–V* curve is in accordance with the measured *I–V* curve.

Root mean square error (RMSE), mean absolute error (MAE), and mean bias error (MBE) are used to evaluate the performance, as shown in the following:

$$\text{RMSE} = \sqrt{\frac{1}{N}\sum_{j=1}^{N}(T_{d,j} - T_{c,j})^2} \tag{41}$$

$$\text{MAE} = \frac{1}{N}\sum_{j=1}^{N}|T_{d,j} - T_{c,j}| \tag{42}$$

$$\text{MBE} = \frac{1}{N}\sum_{j=1}^{N}(T_{d,j} - T_{c,j}) \tag{43}$$

where N is the number of samples, $T_{d,j}$ is the modeling temperature of the jth sample, and $T_{c,j}$ is the measured temperature of the jth sample after calibration.

1) Performance for a Continuous Period of Time: An individual cell in the PV module is half shaded from 11:15 to 12:30 on January 1, 2021. There are no clouds blocking the sun during this continuous period of time. Solar irradiance and ambient temperature during this period of time is steady, as shown in Fig. 11(a). The wind speed parallel to the surface of PV modules during this period of time fluctuates greatly, as shown in Fig. 11(b). Instantaneous, 2-min mean and 10-min mean records of wind speed are available from the environment monitoring recorder described in Section III-A. The current and voltage of the PTS module vary slightly, as shown in Fig. 11(c). In our PV system, every ten modules are connected in series, and their current is dynamically regulated by the inverter (dc–ac).

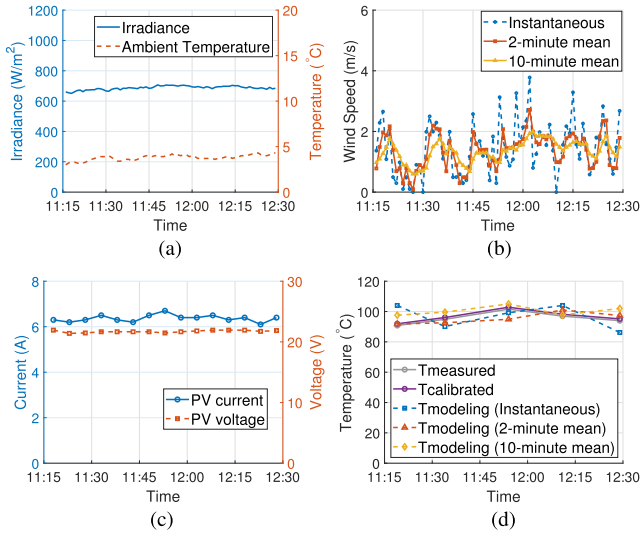

Fig. 11. Performance for a continuous period of time: (a) irradiance and ambient temperature; (b) wind speed parallel to the surface of PV modules; (c) current and voltage of the PTS module; and (d) maximum temperature on the front surface of the PTS module.

TABLE IX
PERFORMANCE EVALUATION FOR THE CONTINUOUS PERIOD OF TIME

	Wind Speed Records	RMSE (°C)	MAE (°C)	MBE (°C)
Tmax	Instantaneous	7.86	7.29	**-0.13**
	2-minute mean	**4.20**	**3.32**	-1.29
	10-minute mean	4.39	3.72	3.57

However, relative to the change of irradiance, there are some lags in the regulation process of inverter. As a result, the current of the PTS module and the irradiance along the time of the day are not completely consistent. Maximum temperature on the front surface of the PTS module is measured with the thermographic camera, calibrated, and also calculated by modeling with instantaneous, 2-min mean and 10-min mean records of wind speed, as shown in Fig. 11(d).

Since the wind speed fluctuates dramatically, the modeling results among instantaneous, 2-min mean and 10-min mean records differ obviously in Fig. 11(d). Performance evaluation for the period of time is shown in Table IX. RMSE and MAE of 2-min mean wind speed records are lower compared with instantaneous records and 10-min mean records. As a tradeoff between real time and steady ability, 2-min mean wind speed records are more suitable to estimate the temperature of PV module.

2) Performance for Various Shading Proportions and Environmental Conditions: One specific cell in the PV module is partially shaded in different proportions, and experiments are conducted under various environmental conditions from December 17, 2020 to January 9, 2021. The ranges of shading proportion, solar irradiance, ambient temperature, and wind speed parallel to the surface of PV modules are listed in Table X. Distributions of the samples are shown in Fig. 12.

Maximum temperature on the front surface of the PTS module is measured with the thermographic camera, calibrated, and also calculated by modeling with 2-min mean wind speed records,

TABLE X
RANGES OF SHADING PROPORTION AND ENVIRONMENTAL CONDITION

Shading Proportion	Irradiance	Ambient Temperature	Wind Speed
25%-75%	587-748 W/m^2	2.8-10.2 °C	0.7-3.8 m/s

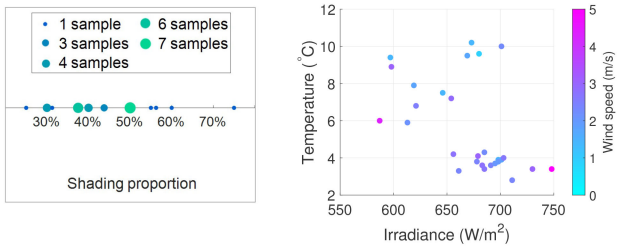

(a) (b)

Fig. 12. Sample distribution: (a) distribution of shading proportion and sample number; (b) distribution of irradiance, temperature, and wind speed parallel to the surface of PV modules.

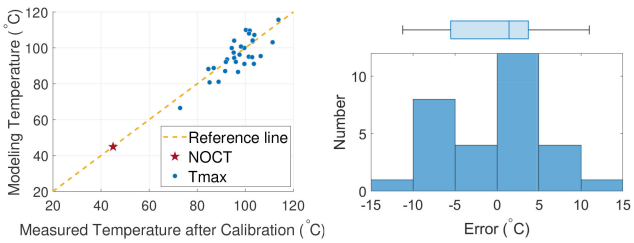

(a) (b)

Fig. 13. Performance for various shading proportions and environmental conditions: (a) comparison of modeling temperation and measured temperature after calibration; and (b) histogram and boxchart of error.

as shown in Fig. 13(a). The modeling Nominal Operation Cell Temperature (NOCT) is 44.9 °C, which is 0.1 °C less than the value given by the datasheet. The sample points are close to the reference line, which implies that the modeling temperature is roughly consistent with the measured temperature. The histogram and boxchart of error is shown in Fig. 13(b).

RMSE, MAE, and MBE of these samples are 6.14 °C, 5.05 °C, and −1.18 °C, respectively. According to the experimental results, the proposed method for temperature estimation of PTS modules performs well.

IV. DISCUSSION

The proposed model has been verified to be effective in the last section. Then some interesting observations are discussed in this section. The temperature distribution of the PTS module corresponding to Fig. 10 is calculated using the proposed method with 2-min mean wind speed record. The infrared thermal images in Fig. 10(b) and (c) are collected almost at the same time. The estimated temperature of glass, TPT, and silicon layer is shown in Fig. 14.

The maximum temperature of the front surface is measured to be 91.9 °C, calibrated to be 93.7 °C, and calculated to be 96.4 °C. The maximum temperature of the back surface is measured to be 95.7 °C, calibrated to be 94.8 °C and calculated to be 98.3 °C. The maximum temperature of the silicon cell is calculated to be 102.0 °C. It is found that the temperature of glass cover is slightly

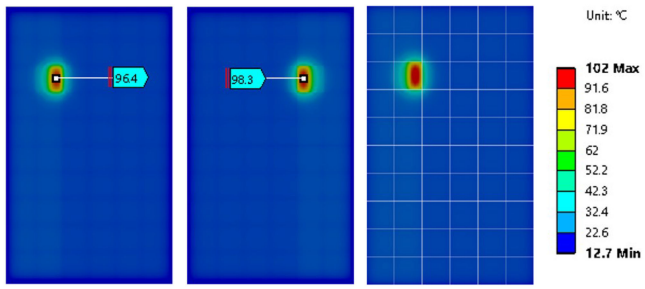

(a) (b) (c) (d)

Fig. 14. Estimated temperature of PTS module: (a) glass cover (front view); (b) TPT (back view); (c) silicon cell (front view); and (d) temperature scale.

lower than the temperature of TPT because of heat conduction. For the same reason, the temperature of the silicon cell is slightly higher than the temperature of glass and TPT.

It also can be observed that the temperature of the unshaded region in the PTS cell is obviously higher than the temperature of the shaded region. When one specific cell in the PV module is partially shaded, this cell might be reverse biased. The current per unit volume of the unshaded region is larger than that of the shaded region in the PTS cell in Fig. 5(a), which means that the unshaded region consume more electricity and generate more heat per unit volume. As a result, the unshaded part of the cell reaches the highest temperature. Due to heat conduction of the silicon cell, the temperature of the shaded part would become higher if it is close to the unshaded part. The heat generation of the shaded region per unit volume is a little more than normal cells. Therefore, the temperature of shaded region is higher than the temperature of normal cells.

V. CONCLUSION

In this aticle, a multiphysics model is developed to estimate the temperature distribution of PTS module. This multiphysics model consists of an electrical model, an optical model, and a thermal model. Particularly, the physically explicable parallel circuit is adopted for the PTS cell, making it possible to estimate the electric power and heat generation of shaded region and unshaded region, respectively. To the best of our knowledge, it is the first attempt to estimate the temperature distribution of PTS module, which can explain the temperature difference between shaded region and unshaded region in the PTS cell. Experiments are conducted on the monocrystalline PV module with area-measurable shade cloth. An individual cell in the PV module is partially shaded with fixed proportion for a continuous period of time on a sunny day. In addition, one specific cell in the PV module is partially shaded in various proportions and environmental conditions. These experimental results verify the effectiveness of the proposed method for temperature estimation of PTS modules. In future research work, more experiments would be conducted to estimate temperature in more complex situations: Multiple cells in the PV module might be partially shaded, and the shading materials with different optical/thermal properties might be considered. Furthermore, the structure model could join the proposed multiphysics model to analyze the thermomechanical stress of the PTS cell.

REFERENCES

[1] A. Gholami *et al.*, "Photovoltaic potential assessment and dust impacts on photovoltaic systems in Iran: Review paper," *IEEE J. Photovolt.*, vol. 10, no. 3, pp. 824–837, May 2020.

[2] E. Piccoli, A. Dama, A. Dolara, and S. Leva, "Experimental validation of a model for PV systems under partial shading for building integrated applications," *Sol. Energy*, vol. 183, pp. 356–370, 2019.

[3] S. Ghosh, V. K. Yadav, and V. Mukherjee, "Evaluation of cumulative impact of partial shading and aerosols on different PV array topologies through combined Shannon's entropy and DEA," *Energy*, vol. 144, pp. 765–775, 2018.

[4] S. Fan, Y. Wang, S. Cao, T. Sun, and P. Liu, "A novel method for analyzing the effect of dust accumulation on energy efficiency loss in photovoltaic (PV) system," *Energy*, vol. 234, 2021, Art. no. 121112.

[5] X. Zhang *et al.*, "Memetic reinforcement learning based maximum power point tracking design for PV systems under partial shading condition," *Energy*, vol. 174, pp. 1079–1090, 2019.

[6] L. Zhu, Q. Li, M. Chen, K. Cao, and Y. Sun, "A simplified mathematical model for power output predicting of building integrated photovoltaic under partial shading conditions," *Energy Convers. Manage.*, vol. 180, pp. 831–843, 2019.

[7] C. E. Clement, J. P. Singh, E. Birgersson, Y. Wang, and Y. S. Khoo, "Hotspot development and shading response of shingled PV modules," *Sol. Energy*, vol. 207, pp. 729–735, 2020.

[8] C. G. Lee *et al.*, "Analysis of electrical and thermal characteristics of PV array under mismatching conditions caused by partial shading and short circuit failure of bypass diodes," *Energy*, vol. 218, 2021, Art. no. 119480.

[9] S. P. Aly, S. Ahzi, N. Barth, and A. Abdallah, "Using energy balance method to study the thermal behavior of PV panels under time-varying field conditions," *Energy Convers. Manage.*, vol. 175, pp. 246–262, 2018.

[10] S. Regondi, H. Hanifi, and J. Schneider, "Modeling and simulation of the influence of interconnection losses on module temperature in moderate and desert regions," *IEEE J. Photovolt.*, vol. 9, no. 5, pp. 1449–1455, Sep. 2019.

[11] M. Libra, T. Petrik, V. Poulek, I. I. Tyukhov, and P. Kourim, "Changes in the efficiency of photovoltaic energy conversion in temperature range with extreme limits," *IEEE J. Photovolt.*, vol. 11, no. 6, pp. 1479–1484, Nov. 2021.

[12] M. C. C. de Oliveira, A. S. A. Diniz Cardoso, M. M. Viana, and V. d. F. C. Lins, "The causes and effects of degradation of encapsulant ethylene vinyl acetate copolymer (EVA) in crystalline silicon photovoltaic modules: A review," *Renewable Sustain. Energy Rev.*, vol. 81, pp. 2299–2317, 2018.

[13] M. Simon and E. L. Meyer, "Detection and analysis of hot-spot formation in solar cells," *Sol. Energy Mater. Sol. Cells*, vol. 94, no. 2, pp. 106–113, 2010.

[14] U. Eitner, S. Kajari-Schröder, M. Köntges, and H. Altenbach, "Thermal stress and strain of solar cells in photovoltaic modules," *Adv. Struct. Mater.*, vol. 15, pp. 453–468, 2011.

[15] J. Zaraket, M. Aillerie, C. Salame, and E. Losson, "Output voltage changes in PV solar modules after electrical and thermal stresses. Experimental analysis," *Energy Procedia*, vol. 157, pp. 1404–1411, 2019.

[16] M. Köntges *et al.*, "Review of failures of photovoltaic modules," Int. Energy Agency, Tech. Rep., 2014.

[17] D. L. King, W. E. Boyson, and J. A. Kratochvil, "Photovoltaic array performance model," Sandia Nat. Lab., Tech. Rep., 2004.

[18] E. Skoplaki and J. A. Palyvos, "Operating temperature of photovoltaic modules: A survey of pertinent correlations," *Renewable Energy*, vol. 34, no. 1, pp. 23–29, 2009.

[19] J. Kurnik, M. Jankovec, K. Brecl, and M. Topic, "Outdoor testing of PV module temperature and performance under different mounting and operational conditions," *Sol. Energy Mater. Sol. Cells*, vol. 95, no. 1, pp. 373–376, 2011.

[20] C. Li, S. V. Spataru, K. Zhang, Y. Yang, and H. Wei, "A multi-state dynamic thermal model for accurate photovoltaic cell temperature estimation," *IEEE J. Photovolt.*, vol. 10, no. 5, pp. 1465–1473, Sep. 2020.

[21] C. F. Abe, J. B. Dias, P. Poggi, and B. Pillot, "Combining identification and translation methods of the single-diode model to compute the average temperature of photovoltaic modules from the open-circuit voltage," *IEEE J. Photovolt.*, vol. 9, no. 5, pp. 1398–1404, Sep. 2019.

[22] M. Munoz Escribano *et al.*, "Module temperature dispersion within a large PV array: Observations at the Amareleja PV plant," *IEEE J. Photovolt.*, vol. 8, no. 6, pp. 1725–1731, Nov. 2018.

[23] J. Zhou, Q. Yi, Y. Wang, and Z. Ye, "Temperature distribution of photovoltaic module based on finite element simulation," *Sol. Energy*, vol. 111, pp. 97–103, 2015.

[24] M. Usama Siddiqui, A. F. Arif, L. Kelley, and S. Dubowsky, "Three-dimensional thermal modeling of a photovoltaic module under varying conditions," *Sol. Energy*, vol. 86, no. 9, pp. 2620–2631, 2012.

[25] M. U. Siddiqui and A. F. Arif, "Electrical, thermal and structural performance of a cooled PV module: Transient analysis using a multiphysics model," *Appl. Energy*, vol. 112, pp. 300–312, 2013.

[26] Q. Li, L. Zhu, Y. Sun, L. Lu, and Y. Yang, "Performance prediction of building integrated photovoltaics under no-shading, shading and masking conditions using a multi-physics model," *Energy*, vol. 213, 2020, Art. no. 118795.

[27] P. Bharadwaj and V. John, "Subcell modeling of partially shaded photovoltaic modules," *IEEE Trans. Ind. Appl.*, vol. 55, no. 3, pp. 3046–3054, May/Jun. 2019.

[28] Y. Shen *et al.*, "Modeling of photovoltaic modules under common shading conditions," *SSRN Electron. J.*, 2021, doi: 10.2139/ssrn.3911164.

[29] G. Petrone, C. A. Ramos-Paja, and G. Spagnuolo, *Photovoltaic Sources Modeling*. Hoboken, NJ, USA: Wiley-IEEE Press, 2017.

[30] C. Li, Y. Yang, S. Spataru, K. Zhang, and H. Wei, "A robust parametrization method of photovoltaic modules for enhancing one-diode model accuracy under varying operating conditions," *Renewable Energy*, vol. 168, pp. 764–778, 2021.

[31] W. Tao, *Heat Transfer*, 5th ed. Beijing, China: Higher Education Press, 2019.

[32] G. Notton, C. Cristofari, M. Mattei, and P. Poggi, "Modelling of a double-glass photovoltaic module using finite differences," *Appl. Thermal Eng.*, vol. 25, no. 17–18, pp. 2854–2877, 2005.